

LMNet: Real-time Multiclass Object Detection on CPU using 3D LiDAR

Kazuki Minemura¹, Hengfui Liao¹, Abraham Monrroy² and Shinpei Kato³
{kazuki.minemura, heng.hui.liao}@intel.com, amonrroy@ertl.jp, shinpei@is.s.u-tokyo.ac.jp

Abstract—This paper describes an optimized single-stage deep convolutional neural network to detect objects in urban environments, using nothing more than point cloud data. This feature enables our method to work regardless the time of the day and the lighting conditions. The proposed network structure employs dilated convolutions to gradually increase the perceptive field as depth increases, this helps to reduce the computation time by about 30%. The network input consists of five perspective representations of the unorganized point cloud data. The network outputs an objectness map and the bounding box offset values for each point. Our experiments showed that using reflection, range, and the position on each of the three axes helped to improve the location and orientation of the output bounding box. We carried out quantitative evaluations with the help of the KITTI dataset evaluation server. It achieved the fastest processing speed among the other contenders, making it suitable for real-time applications. We implemented and tested it on a real vehicle with a Velodyne HDL-64 mounted on top of it. We achieved execution times as fast as 50 FPS using desktop GPUs, and up to 10 FPS on a single Intel Core i5 CPU. The deploy implementation is open-sourced and it can be found as a feature branch inside the autonomous driving framework Autoware. Code is available at: https://github.com/CPFL/Autoware/tree/feature/cnn_lidar_detection

I. INTRODUCTION

Automated driving can bring significant benefits to human society. It can ameliorate accidents on the road, provide mobility to persons with reduced capacities, automate delivery services, help the elderly to safely move between places, among many others.

Deep Learning has been applied successfully to detect objects with great accuracy on point cloud. Previous work on this area, used similar techniques taken from the work on Convolutional Neural Networks for object detection on images (e.g., 3D-SSMFCNN [1]), and extended its use on point cloud projections. To name some: F-pointNet [2], VoxelNet [3], AVOD [4], DoBEM [5], MV3D [6], among others. However, none of these are capable to perform on real-time scenarios. These approaches will be examined further in Section II.

Knowing that point cloud can be treated as an image (if projecting it to a 2D plane) and exploit the powerful deep learning techniques from CNNs to detect objects on it, we propose a 3D LiDAR-based multi-class object detection

network (LMNet). Our network aims to achieve real-time performance, so it can be applied to automated driving systems. In contrast to other approaches, such as MV3D, which uses multiple inputs: Top and Frontal projections, and RGB data taken from a camera. Ours adopts a single-stage strategy from a single point cloud. LMNet also employs a custom designed layer for dilated convolutions. This extends the perception regions, conducts pixel-wise segmentation and fine-tunes 3D bounding box prediction. Furthermore, combining it with a dropout strategy [7] and data augmentation, our approach shows significant improvements in runtime and accuracy. The network can perform oriented 3D box regression, to predict location, size and orientation of objects in 3D space.

The main contributions of this work are:

- To design a CNN capable to achieve real-time like 3D multi-class object detection using only point cloud data on real-time on CPU.
- To implement, test our work in a real vehicle.
- To enable multi-class object detection in the same network (Vehicle, Pedestrian, Bike or Bicycle, as defined in the KITTI dataset).
- To open-source the pre-trained models and inference code.

As for the evaluation of the 3D Object detection, we use the KITTI dataset [8] evaluation server to submit and get a fair comparison. Experimental results suggest that LMNet can detect multi-class objects with certain accuracy for each category while achieving up to 50 FPS on GPU. Performing better than those of DoBEM and 3D-SSMFCNN.

The structure of this paper is as follows: Section II introduces the state-of-the-art architectures. Section III details the input encoding and the LMNet. Section IV describes the network outputs, compares with other state-of-the-art architectures, and shows the tests on a real vehicle. Finally, we summarize and conclude in the Section V.

II. RELATED WORK

Previous research has focused primarily on improving the accuracy of the object detection. Thanks to this, great progress has been made in this field. However, these approaches leave performance out of the scope. In this section, we present our findings on the current literature and analyze how to improve performance.

While surveying current work in this field, we found out that object detection on LiDAR data can be classified into three main different methods to handle the point cloud: a)

¹ Kazuki Minemura and Hengfui Liao are with Intel's Internet of Things Group, Bayan Lepas, 11900, Penang, Malaysia.

² Abraham Monrroy is with Nagoya University, Parallel and Distributed Systems lab, Nagoya, Furo-cho, 464-8601, Aichi, Japan.

³ Shinpei Kato is Associate Professor at the School of Science for The University of Tokyo, Bunkyo-ku, 113-0033, Tokyo, Japan.

TABLE I
IMPLEMENTED DILATED LAYERS

Layer	1	2	3	4	5	6	7	8
Kernel size	3×3	3×3	3×3	3×3	3×3	3×3	3×3	1×1
Dilation	1	1	2	4	8	16	32	N/A
Receptive filed	3×3	3×3	7×7	15×15	31×31	63×63	127×127	127×127
Feature channels	128	128	128	128	128	128	128	64
Activation function	Relu	Relu	Relu	Relu	Relu	Relu	Relu	Relu

direct manipulation of raw 3D coordinates, b) point cloud projection and application of Fully Convolutional Networks, and c) Augmentation of the perceptive fields from previous approach using dilated convolutions.

A. Manipulation of 3D coordinates

Within this class, we can find noteworthy mentions: PointNet [9], PointNet++ [10], F-PointNet [2], VoxelNet, VeloFCN [11], and MV3D. Being PointNet the pioneer on this group and can be further classified into three sub-groups.

The first group is composed of PointNet and its variants. These methods extract point-wise features from raw point cloud data. Pointnet++ was developed on top of PointNet to handle object scaling. Both PointNet and PointNet++ have shown to work reliably well in indoor environments. More recently, F-Pointnet was developed to enable road object detection in urban driving environments. This method relies on an independent image-based object detector to generate high-quality object proposals. The point cloud within the proposal boxes is extracted and fed onto the point-wise based object detector, this helps to improve detection results on ideal scenarios. However, F-PointNet uses two different input sources, cannot be trained in an end-to-end manner, requiring the image based proposal generator to be independently trained. Additionally, this approach showed poor performance when image data from low-light environments were used to get the proposals, making it difficult to deploy on real application scenarios.

The second group of methods is Voxel based. VoxelNet [3] divides the point cloud scene into fixed size 3D Voxel grids. A noticeable feature is that VoxelNet directly extracts the features from the raw point cloud in the 3D voxel grid. This method scored remarkably well in the KITTI benchmark.

Finally, the last group of popular approaches is 2D based methods. VeloFCN was the first one to project the point cloud to an image plane coordinate system. Exploiting the lessons learned from the image based CNN methods, it trained the network using the well-known VGG16 [12] architecture from Oxford. On top this feature layers, it added a second branch to the network to regress the bounding box locations. MV3D, an extended version of VeloFCN, introduced multi-view representations for point cloud by incorporating features from bird and frontal-views.

Generally speaking, 2D based methods have shown to be faster than those that work directly on 3D space. With speed in mind, and due to the constraint we previously set of using nothing more than LiDAR data, we decided to implement LMNet as a 2D based method. This not only allows LMNet

to perform faster, but it also enables it to work on low-light scenarios, since it is not using RGB data.

B. Fully Convolutional Networks

FCN have demonstrated state-of-the-art results in several semantic segmentation benchmarks (e.g., PASCAL VOC, MSCOCO, etc.), and object detection benchmarks (e.g., KITTI, etc.). The key idea of many of these methods is to use feature maps from pre-trained networks (e.g., VG-GNet) to form a feature extractor. SegNet [13] initially proposed an encoder-decoder architecture for semantic segmentation. During the encoding stage, the feature map is down-sampled and later up-sampled using an unpooling layer [13]. DeepLabV1 [14] increases the receptive field at each layer using dilated convolution filter.

In this work, the 3D point cloud is represented as a plane that extracts the shape and depth information. Using this procedure, an FCN can be trained from scratch using the KITTI dataset data or its derivatives (e.g., data augmentation). This also enables us to design a custom network, and be more flexible while addressing the segmentation problem at hand. For instance, we can integrate a similar encoder-decoder technique as the one described in SegNet. More specifically, LMNet is designed to have larger perceptive fields, quickly process larger resolution feature maps, and simultaneously validate the segmentation accuracy [15].

C. Dilated convolution

Traditional convolution filter limits the perceptive field to uniform kernel sizes (e.g., 3×3 , 5×5 , etc). An efficient approach to expanding the receptive field, while keeping the number of parameters and layers small, is to employ the dilated convolution. This technique enables an exponential expansion of the receptive field while maintaining resolution [16], [17] (e.g., the feature map size can be as big same as the input size). For this to work effectively, it is important to restrict the number of layers to reduce the FCN’s memory requirements. This is especially true when working with higher resolution feature maps. Dilated convolutions are widely used in semantic segmentation on images. To the best of our knowledge, LMNet is the first network that uses dilated convolution filter on point cloud data to detects objects.

Table I shows the implemented dilated layers in LMNet. The dilated convolution layer is larger than the input features maps, which have a size of 64×512 pixels. This allows the FCN to access a larger context window to refer road objects. For each dilated convolution layer, a dropout layer

TABLE II

SUMMARY OF NETWORK ARCHITECTURES WITH INPUT DATA, DETECTION TYPE, SOURCE CODE AVAILABILITY AND INFERENCE TIME.

Network	Input Data	Class	Code	Inference
F-pointNet [2]	Image and Lidar	multi	Yes	170ms
VoxelNet [3]	Lidar	multi	N/A	30ms
AVOD [4]	Image and Lidar	multi	Yes	80ms
MV3D [18]	Image and Lidar	car	Yes	350ms
DoBEM [5]	Image and Lidar	car	N/A	600ms
3D-SSMFCNN [1]	Image	car	Yes	100ms

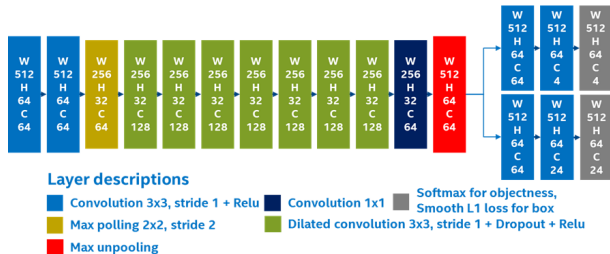


Fig. 1. LMNet architecture

is added between convolution and ReLU layers to regularize the network and avoid over-fitting.

D. Comparison

As this work aims to design a fast 3D multi-class object detection network, we mainly compare with other previously published 3D object detection networks: F-pointNet, VoxelNet, AVOD, MV3D, DoBEM, and 3D-SSMFCNN.

To have a basic overview of the previously mentioned networks, Table II lists the items: (a) Data, which is what data feed in to the network; (b) type, which is detection availability (i.e. multi-class, car only); (c) Code, which is code availability, and; (d) Inference, which is the time taken to forward the input data and generate outputs.

Although, some of state-of-the-art network source code (viz., F-pointNet, AVOD) are available, the models reported to Kitti are not available. We can only infer that by the type of data being fed, the outlined accuracy, and the manually reported inference time. Additionally, none of them are capable to be processed in real-time (more than 30 FPS) [19]. A third party, Boston Didi team, implemented the MV3D model [18]. This method can only perform single class detection and would not be suitable to perform a comparison. Furthermore, the reported inference performance is less than 3 FPS. For the previous reasons, we firmly believe that open sourcing a fast object detection method and its corresponding inference code can greatly contribute to the development of faster and highly accurate detectors in the automated driving community.

III. PROPOSED ARCHITECTURE

The proposed network architecture takes as input five representations of the frontal-view projection of a 3D point cloud. These five input maps help the network to keep 3D information at hand. The architecture outputs an objectness map and 3D bounding box offset values calculated directly from the frontal-view map. The objectness map contains

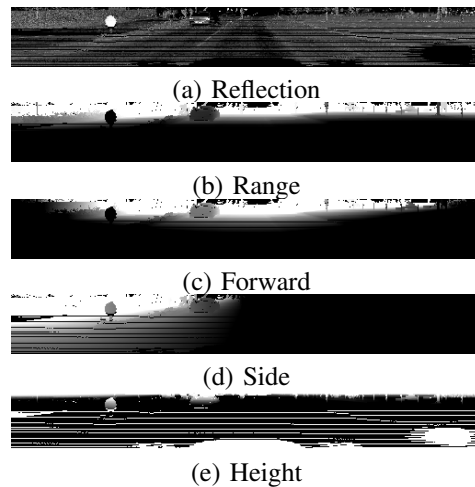


Fig. 2. Encoded input point cloud

the class confidence values for each of the projected 3D points. The box candidates calculated from the offset values are filtered using a custom euclidean distance based non-maximum suppression procedure. A diagram of the proposed network architecture can be visualized in Fig. 1.

Albeit frontal-view representations [20] have less information than bird-view [6], [16] representations or raw-point [9], [10] data. We can expect less computational cost and certain detection accuracy [21].

A. Frontal-view representation

To obtain a sparse 2D point map, we employ a cylindrical projection [20]. Given a 3D point $p = (x, y, z)$. Its corresponding coordinates in the frontal-view map $p_f = (r, c)$ can be calculated as follows:

$$c = \lfloor \text{atan2}(y, x) / \delta\theta \rfloor, \quad (1)$$

$$r = \lfloor \text{atan2}(z, \sqrt{x^2 + y^2}) / \delta\phi \rfloor. \quad (2)$$

where $\delta\theta$ and $\delta\phi$ are the horizontal and vertical resolutions (e.g., 0.32 and 0.4 while 0.08, 0.4 radian in Velodyne HDL-64E [22]) of the LiDAR sensor, respectively.

Using this projection, five feature channels are generated:

- 1) Reflection, which is the normalized value of the reflectivity as returned by the laser for each point.
- 2) Range, which is the distance on the XY plane (or the ground) of the sensor coordinate system. It can be calculated as $\sqrt{x^2 + y^2}$.
- 3) The distance to the front of the car. Equivalent to the x coordinate on the LiDAR frame.
- 4) Side, the y coordinate value on the sensor coordinate system. Positive values represent a distance to the left, while negative ones depict points located to the right of the vehicle.
- 5) Height, as measured from the sensor location. Equal to the z coordinate as shown in Fig. 2.

B. Bounding Box Encoding

As for the bounding boxes, we follow the encoding approach from [20], which considers the offset of corner

points and its rotation matrix. There are two reasons on why to use this approach as shown in Ref [20]: (A) A faster CNN convergence due to the reduced offset distribution leading to a smaller regression search space, and (B) Enable rotation invariance. We briefly describe the encoding in this section.

Assuming a LiDAR point $p = (x, y, z) \in P$, an object point and a background point can be represented as $p \in O$, $p \in O^c$, respectively. The box encoding considers the points forming the objects, e.g., $p \in O$. The observation angles (e.g., azimuth and elevation) are calculated as follows:

$$\theta = \text{atan2}(y, x), \quad (3)$$

$$\phi = \text{atan2}(z, \sqrt{x^2 + y^2}). \quad (4)$$

Therefore, the rotation matrix R can be defined as follows,

$$R = R_z(\theta)R_y(\phi). \quad (5)$$

where $R_z(\theta)$ and $R_y(\phi)$ are the rotation functions around the z and y axes, respectively. Then, the i -th bounding box corner $c_{p,i} = (x_{c,i}, y_{c,i}, z_{c,i})$ can be encoded as:

$$c'_{p,i} = R^T(c_{p,i} - p). \quad (6)$$

Our proposed architecture regress c'_p during training. The eight corners of a bounding box are concatenated in a 24-d vector as,

$$b'_p = (c'^T_{p,1}, c'^T_{p,2}, c'^T_{p,3}, \dots, c'^T_{p,8})^T. \quad (7)$$

Thus, the bounding box output map has 24 channels with the same resolution as the input one.

C. Proposed Architecture

The proposed CNN architecture is similar to LoDNN [16]. As illustrated in Fig. 1, the CNN feature map is processed by two 3×3 convolution, eight dilated convolution and followed by 3×3 and 1×1 convolution layers. The trunk splits at the max-pooling layer into the objectness classification branch and the bounding box's corners offset regression branch. We use $(d)\text{conv}(c_{in}, c_{out}, k)$ to represent a 2-dimensional convolution/dilated-convolution operator where c_{in} is the number of input channel, and c_{out} is the number of output channels, k represent the kernel size, respectively.

A five-channel map of size of $64 \times 512 \times 5$, as described in Section 2, are fed into an encoder with two convolution layers, $\text{conv}(5, 64, 3)$ and $\text{conv}(64, 64, 3)$. These are followed by a max-pooling layer to the output of the encoder, this helps to reduce FCN's memory requirements as previously mentioned.

The encoder section is succeeded by seven dilated-convolutions [17] (see dilation parameters in Table I) and a convolution, e.g., $d\text{conv}_1(64, 128, 3)$; $d\text{conv}_{2-7}(128, 128, 3)$; and $\text{conv}(128, 64, 1)$, with a dropout layer and a rectified linear unit (ReLU) activation applied to the pooled feature map, enabling the layer to extract multi-scale contextual information.

Following the context module, the main trunk bifurcates to create the objectness and corners branches. Both of them have a decoder that up-samples the feature map, from the dilated convolutions to the same size as the input. This is achieved with the help of a max-unpooling layer [13], followed by two convolution layers: $\text{conv}(64, 64, 3)$ with ReLU, and; $\text{conv}(64, 4, 3)$ with ReLU for objectness branch, or $\text{conv}(64, 24, 3)$ for corners branch.

The objectness branch outputs an object confidence map, while the corners-branch generates the corner-points offsets. Softmax loss is employed to calculate the objectness loss between the confidence map and the encoded objectness map. Finally, Smooth l_1 [23] is utilized for the corner offset regression loss between the corners offset and ground truth corners offset.

To train a multi-task network, a re-weighting approach is employed as explained in Ref [20] to balance the objective of learning both objectness map and bounding box's offset values. The multi-task function L can be defined as follows:

$$L = \sum_{p \in P} w_{obj}(p)L_{obj}(p) + \sum_{p \in O} w_{cor}(p)L_{cor}(p), \quad (8)$$

where L_{obj} and L_{cor} denote the softmax loss and regression loss of point p , respectively, while w_{obj} and w_{cor} are point-wise weights, e.g., objectness weight and corners weight, calculated by the following equations:

$$w_{cor}(p) = \begin{cases} \bar{s}[\kappa_p]/s(p) & p \in O, \\ 1 & p \in O^c, \end{cases} \quad (9)$$

$$w_{bac}(p) = \begin{cases} m|O|/|O^c| & p \in O^c, \\ 1 & p \in O, \end{cases} \quad (10)$$

$$w_{obj}(p) = w_{bac}(p)w_{cor}(p), \quad (11)$$

where $\bar{s}[x]$ is the average shape size of the class $x \in \{\text{car, pedestrian, cyclist}\}$, κ_p denotes point p class, $s(p)$ represents the size of an object which the point p belongs to, $|O|$ denotes the number of points on all objects, $|O^c|$ denotes the number of points on the background. In a point cloud scene, most of the points are corresponding to the background. A constant weight, m , is introduced to balances the softmax losses between the foreground and the background object. Empirically, m is set to 4.

D. Training Phase

The KITTI dataset only has annotations for objects in the frontal-view on the camera image. Thus, we limit point cloud range in $[0, 70] \times [-40, 40] \times [-2, 2]$ meters, and ignore the points in out of image boundaries after projection (see Section III-A). Since KITTI uses the Velodyne HDL64E, we obtain a 64×512 map for the frontal-view maps.

The proposed architecture is implemented using Caffe [24], while adding the custom unpooling layers implementations. The network is trained in an end-to-end manner using stochastic gradient decent (SGD) algorithm with a learning rate of 10^{-6} for 200 epoch for our dataset. The batch size is set to 4.

TABLE III
PERFORMANCE BOARD

Newtwork	Accelerator	Inference	Car	Ped.	Cyc.
F-PointNet [2]	GTX 1080	88ms	70.39	44.89	56.77
VoxelNet (Lidar) [3]	Titan X	30ms	65.11	33.69	48.36
AVOD [4]	Titan Xp	80ms	65.78	31.51	44.90
MV3D [6]	Titan X	360ms	63.35	N/A	N/A
MV3D (Lidar) [6]	Titan X	240ms	52.73	N/A	N/A
DoBEM [5]	Titan X	600ms	6.95	N/A	N/A
3D-SSMFCNN [1]	Titan X	100ms	2.28	N/A	N/A
Proposed	GTX 1080	20ms	15.24	11.46	3.23

E. Data augmentation

The number of point cloud samples in the KITTI training dataset is 7481, which is considerably less than other image datasets (e.g., ILSVRC [25], has 456567 images for training). Therefore, data augmentation technique is applied to avoid overfitting, and to improve the generalization of our model. Each point cloud cluster that is corresponding to an object class was randomly rotating at LiDAR z -axis $[-15^\circ, 15^\circ]$. Using the proposed data augmentation, the training set dramatically increased to more than 20000 data samples.

F. Testing Phase

The objectness map includes a non-object class and the corner map may output many corner offsets. Consider the corresponding corner points $\{c_{p,i}|i \in 1, \dots, 8\}$ by the inverse transform of Eq. 6. Each bounding box candidates can be denoted by $b_p = (c_{p,1}^T, c_{p,2}^T, c_{p,3}^T, \dots, c_{p,8}^T)^T$. The sets of all box candidates is $B = \{b_p | p \in obj\}$.

To reduce bounding boxes redundancy, we apply a modified non-maximum suppression (NMS) algorithm, which selects the bounding box based on the euclidean distance between the front-top-left and rear-bottom-right corner points of the box candidates. Each box b_p is scored by counting its neighbor bounding boxes in B within distance $\delta_{car}, \delta_{pedestrian}, \delta_{cyclist}$, denoted as $\#\{\|c_{p_i,1} - c_{p_j,1}\| + \|c_{p_i,8} - c_{p_j,8}\| < \delta_{class}\}$. Then, the bounding boxes B are sorted by descending score. Afterwards, the bounding box candidates whose score is less than five are discarded as outliers. Picking up a box who has the highest score in B , the euclidean distances between the box and the rest are calculated. Finally, the boxes whose distance are less than the predefined threshold values are removed. The empirically obtained thresholds for each class are: (a) $T_{car} = 0.7m$; (b) $T_{pedestrian} = 0.3m$, and; (c) $T_{cyclist} = 0.3m$.

IV. EXPERIMENTS

The evaluation results of LMNet on the challenging KITTI object detection benchmark [8] are shown in this section. The benchmark provides image and point cloud data, 7481 sets for training and 7518 sets for testing. LMNet is evaluated on KITTI's 2D, 3D and bird view object detection benchmark using online evaluation server.

A. Inference Time

One of the major issue for the application of a 3D object detection network is inference time. We compare the inference time taken by LMNet and some representative

TABLE IV
INFERENCE TIME ON CPU

Caffe version	i5-6600K	E5-2698 v4
Caffe with OpenBlas	351ms	280ms
Intel Caffe with MKL2017	99ms	47ms

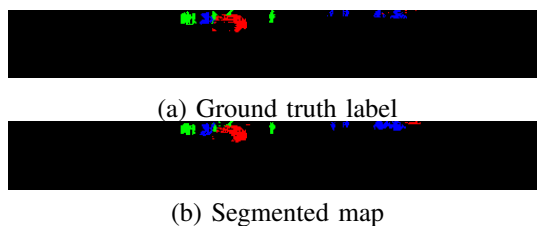


Fig. 3. Ground truth label and segmented map

state-of-art networks. Table III shows inference time on CUDA enabled GPUs of LMNet and other representatives methods. LMNet achieved the fastest inference at 20ms on a GTX 1080. Further tests on a Titan Xp observed inference time of 12ms, and 6.8ms (147 FPS) for Tesla P40. LMNet is the fastest in the wild and enables real-time (30 FPS or better) [19] detection.

B. Towards Real-Time Detection on General Purpose CPU

To test the inference time on CPU, LMNet is using Intel Caffe [26], which is optimized for Intel architecture CPUs through Intel's math kernel library (MKL). For the execution measurements, we include not only the inference time but also the time required to pre-process, project and generate the input data from the point cloud, as well as the post-processing time used to generate the objectness map and bounding box coordinates. Table IV shows that LMNet can achieve more than 10 FPS on an Intel CPU i5-6600K (4 cores, 3.5 GHz) and 20 FPS on Xeon E5-2698 v4 (20 cores, 2.2 GHz). Given that the Lidar scanning frequency is 10 Hz, the 10 FPS achieved by LMNet is considered as real-time. These results are promising for automated driving systems that only use general purpose CPU. LMNet could be deployed to edge devices.

C. Project Map Segmentation

Based on our observations, the trained model at 200 epochs is used for performance evaluation. The obtained segmented map and its corresponding ground truth label from the validation set can be appreciated in Fig. 3. The segmented object confidence map is very similar to the ground truth. Experiment result shows that LMNet can accurately classify points by its class.

D. Object Detection

The evaluation of LMNet was carried out on the KITTI dataset evaluation server. Particularly, multi-class object detection on 2D, 3D and BV categories. Table. III shows the average precision on 3D object detection in the moderate setting. LMNet performed a certain 3D detection accuracies, 15.24% for car, 11.46% for pedestrian and 3.23% for cyclist, respectively. The state-of-art networks achieve more than 50% accuracy for car, 20% for the pedestrian and 29%.

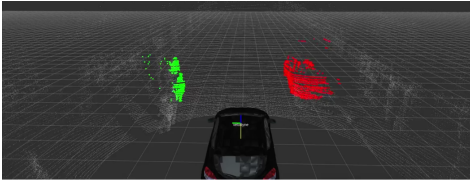


Fig. 4. 3D point cloud classified by LMNet from a Velodyne HDL-64E

MV3D achieved 52% accuracy for car objects. However, those networks are either not executed in real-time, only single class, or not open-sourced as mentioned in the Section II-D. To our best knowledge, LMNet is the fastest multi-class object detection network using data only from LiDAR, with models and code open sourced.

E. Test on real-world data

We implemented LMNet as an Autoware [27] module. Autoware is an autonomous driving framework for urban roads. It includes sensing, localization, fusion and perception modules. We decided to use this framework due to the easiness of installation, its compatibility with ROS [28] and because it is open-source, allowing us to focus only on the implementation of our method. The sensing module allowed us to connect with a Velodyne HDL-64E LiDAR, the same model as the one used in the KITTI dataset. With the help of the ROS, PCL and OpenCV libraries, we projected the sensor point cloud, constructed the five-channel input map as described in III-A, fed them to our Caffe fork and obtained both the output maps. Fig. 4 shows the classified 3D point cloud.

V. CONCLUSIONS

This paper introduces LMNet, a multi-class, real-time network architecture for 3D object detection on point cloud. Experimental results show that it can achieve real-time performance on consumer grade CPUs. The predicted bounding boxes are evaluated on KITTI evaluation server. Although the accuracy is on par with other state-of-the-art architectures, LMNet is significantly faster and able to detect multi-class road objects. The implementation and pre-trained models are open-sourced, so anyone can easily test our claims. Training code is also planned to be open sourced. It is important to note that all the evaluations are using the bounding box location, as defined by the KITTI dataset. However, this does not correctly reflect the classifier accuracy at a point-wise level. As for future work, we intend to fine-tune the bounding box non-maximum suppression algorithm to perform better on the KITTI evaluation; Implement the network on low-power platforms such as the Intel Movidius's Myriad [29] and Atom, to test its capability on a wider range of IoT or embedded solutions.

REFERENCES

- [1] L. Novak, "Vehicle detection and pose estimation for autonomous driving," 2017.
- [2] C. R. Qi, W. Liu, C. Wu, H. Su, and L. J. Guibas, "Frustum pointnets for 3D object detection from RGB-D data," *arXiv preprint arXiv:1711.08488*, 2017.
- [3] Y. Zhou and O. Tuzel, "VoxelNet: end-to-end learning for point cloud based 3D object detection," *arXiv preprint arXiv:1711.06396*, 2017.

- [4] J. Ku, M. Mozifian, J. Lee, A. Harakeh, and S. Waslander, "Joint 3D proposal generation and object detection from view aggregation," *arXiv preprint arXiv:1712.02294*, dec 2017.
- [5] S.-I. Yu, T. Westfechtel, R. Hamada, K. Ohno, and S. Tadokoro, "Vehicle detection and localization on bird's eye view elevation images using convolutional neural network," in *IEEE International Symposium on Safety, Security and Rescue Robotics*, oct 2017, pp. 102–109.
- [6] X. Chen, H. Ma, J. Wan, B. Li, and T. Xia, "Multi-view 3d object detection network for autonomous driving," in *IEEE Conference on Computer Vision and Pattern Recognition*, jul 2017, pp. 6526–6534.
- [7] N. Srivastava, G. Hinton, A. Krizhevsky, I. Sutskever, and R. Salakhutdinov, "Dropout: A simple way to prevent neural networks from overfitting," *The Journal of Machine Learning Research*, vol. 15, no. 1, pp. 1929–1958, Jan. 2014.
- [8] A. Geiger, P. Lenz, and R. Urtasun, "Are we ready for autonomous driving? the kitti vision benchmark suite," in *Conference on Computer Vision and Pattern Recognition*, 2012.
- [9] C. R. Qi, H. Su, K. Mo, and L. J. Guibas, "PointNet: deep learning on point sets for 3D classification and segmentation," *Fourth International Conference on 3D Vision*, pp. 601–610, dec 2016.
- [10] C. R. Qi, L. Yi, H. Su, and L. J. Guibas, "PointNet++: deep hierarchical feature learning on point sets in a metric space," *arXiv preprint arXiv:1706.02413*, jun 2017.
- [11] B. Li, T. Zhang, and T. Xia, "Vehicle detection from 3D lidar using fully convolutional network," in *Robotics: Science and Systems*. Robotics: Science and Systems Foundation, 2016.
- [12] S. Karen and Z. Andrew, "Very deep convolutional networks for large-scale image recognition," *arXiv preprint arXiv:1409.1556*, 2014.
- [13] V. Badrinarayanan, A. Kendall, and R. Cipolla, "SegNet: a deep convolutional encoder-decoder architecture for image segmentation," *IEEE Transactions on Pattern Analysis and Machine Intelligence*, vol. 39, no. 12, pp. 2481–2495, dec 2017.
- [14] L.-C. Chen, G. Papandreou, I. Kokkinos, K. Murphy, and A. L. Yuille, "DeepLab: semantic image segmentation with deep convolutional nets, atrous convolution, and fully connected CRFs," *IEEE Transactions on Pattern Analysis and Machine Intelligence*, pp. 1–1, 2017.
- [15] Z. Wu, C. Shen, and A. van den Hengel, "High-performance semantic segmentation using very deep fully convolutional networks," *arXiv preprint arXiv:1604.04339*, pp. 1–11, 2016.
- [16] L. Caltagirone, S. Scheidegger, L. Svensson, and M. Wahde, "Fast lidar-based road detection using fully convolutional neural networks," in *IEEE Intelligent Vehicles Symposium*, jun 2017, pp. 1019–1024.
- [17] F. Yu and V. Koltun, "Multi-scale context aggregation by dilated convolutions," *arXiv preprint arXiv:1511.07122*, 2015.
- [18] "MV3D code," 2017. [Online]. Available: <https://github.com/bostondiditeam/MV3D>
- [19] M. A. Sadeghi and D. Forsyth, "30Hz object detection with DPM v5," in *European Conference on Computer Vision*, D. Fleet, T. Pajdla, B. Schiele, and T. Tuytelaars, Eds., 2014, pp. 65–79.
- [20] B. Li, T. Zhang, and T. Xia, "Vehicle detection from 3D lidar using fully convolutional network," in *Robotics: Science and Systems*, 2016.
- [21] C. R. Qi, H. Su, M. NieBner, A. Dai, M. Yan, and L. J. Guibas, "Volumetric and multi-view CNNs for object classification on 3D data," in *IEEE Conference on Computer Vision and Pattern Recognition*, jun 2016, pp. 5648–5656.
- [22] "Velodyne HDL-64E lidar sensor." [Online]. Available: <http://velodynelidar.com/hdl-64e.html>
- [23] R. Girshick, "Fast R-CNN," in *IEEE International Conference on Computer Vision*, dec 2015, pp. 1440–1448.
- [24] Y. Jia, E. Shelhamer, J. Donahue, S. Karayev, J. Long, R. Girshick, S. Guadarrama, and T. Darrell, "Caffe: convolutional architecture for fast feature embedding," *arXiv preprint arXiv:1408.5093*, 2014.
- [25] O. Russakovsky, J. Deng, H. Su, J. Krause, S. Satheesh, S. Ma, Z. Huang, A. Karpathy, A. Khosla, M. Bernstein, A. C. Berg, and L. Fei-Fei, "ImageNet large scale visual recognition challenge," *International Journal of Computer Vision*, vol. 115, no. 3, pp. 211–252, 2015.
- [26] "Intelcaffe." [Online]. Available: <https://github.com/intel/caffe>
- [27] S. Kato, E. Takeuchi, Y. Ishiguro, Y. Ninomiya, K. Takeda, and T. Hamada, "An open approach to autonomous vehicles," *IEEE Micro*, vol. 35, no. 6, pp. 60–68, nov 2015.
- [28] M. Quigley, K. Conley, B. P. Gerkey, J. Faust, T. Foote, J. Leibs, R. Wheeler, and A. Y. Ng, "ROS: an open-source robot operating system," in *ICRA Workshop on Open Source Software*, 2009.
- [29] Movidius, "Ins-03510-c1 datasheet," 2014. [Online]. Available: <http://uploads.movidius.com/1441734401-Myriad-2-product-brief.pdf>